Ketogenic Diet Modulates Neuroinflammation via Metabolites from Lactobacillus reuteri after Repetitive Mild Traumatic Brain Injury in Adolescent Mice

Dilirebati Dilimulati
Shanghai Jiao Tong University School of Medicine Affiliated Renji Hospital https://orcid.org/0000-0001-6381-6144

Fengchen Zhang
Shanghai Jiao Tong University School of Medicine Affiliated Renji Hospital

Shuai Shao
Shanghai Jiao Tong University School of Medicine Affiliated Renji Hospital

Tao Lv
Shanghai Jiao Tong University School of Medicine Affiliated Renji Hospital

Qing Lu
Shanghai Jiao Tong University School of Medicine Affiliated Renji Hospital

Mengqiu Cao
Shanghai Jiao Tong University School of Medicine Affiliated Renji Hospital

Yichao Jin (honam612@163.com)
Shanghai Jiao Tong University School of Medicine Affiliated Renji Hospital https://orcid.org/0000-0003-4141-7876

Feng Jia
Shanghai Jiao Tong University School of Medicine Affiliated Renji Hospital

Xiaohua Zhang
Shanghai Jiao Tong University School of Medicine Affiliated Renji Hospital

Research Article

Keywords: Repetitive mild traumatic brain injury, Ketogenic diet, Aryl hydrocarbon receptor, Toll-like receptor, Neuroinflammation

Posted Date: January 28th, 2022

DOI: https://doi.org/10.21203/rs.3.rs-1155536/v1

Abstract

Repetitive mild traumatic brain injury (rmTBI) is associated with a range of neural changes which is characterized by axonal injury and neuroinflammation. Ketogenic diet (KD) is regarded as a potential therapy for facilitating recovery after moderate-severe traumatic brain injury (TBI). However, its effect on rmTBI has not been studied. In this study, we evaluated the anti-neuroinflammation effects of KD after rmTBI in adolescent mice and explored the potential mechanisms. Experimentally, specific pathogen-free (SPF) adolescent male C57BL/6 mice received a sham surgery or repetitive mild controlled cortical impacts consecutively for 7 days. The uninjured mice received the standard diet, and the mice with rmTBI were fed either the standard diet or KD for 7 days. One week later, all mice were subjected to behavioral tests and experimental analysis. Results suggest that KD significantly increased blood beta-hydroxybutyrate (β-HB) levels and improved neurological function. KD also reduced white matter damage, microgliosis and astrogliosis induced by rmTBI. Aryl hydrocarbon receptor (AHR) signaling pathway, which was mediated by indole-3-acetic acid (3-IAA) from *Lactobacillus reuteri* (L. *reuteri*) in gut and activated in the microglia after rmTBI, was inhibited by KD. The expression level of the toll-like receptor 4 (TLR4)/myeloid differentiation primary response 88 (MyD88) in microglial cells, which mediates the NF-κB pathway, was also attenuated by KD. Taken together, our results indicated that KD can promote recovery following rmTBI in adolescent mice. KD may modulate microgliosis and activation by altering L. reuteri in gut and its metabolites. The inhibition of indole/AHR pathway and the downregulation of TLR4/MyD88 may play a role in the beneficial effect of KD against neuroinflammation in rmTBI mice.

Introduction

Repetitive mild traumatic brain injury (rmTBI), also known as brain concussion, is a growing medical and economic problem worldwide, accounting for 70-90% of all traumatic brain injury cases (Maas, Menon et al. 2017). rmTBI might increase the long-term risk for cognitive impairment and dementia, stroke, Parkinson disease, and epilepsy, and is associated with increased long-term mortality rates(Maas, Menon et al. 2017). Emerging evidence suggests that rmTBI is associated with histopathological changes such as astrogliosis, microglial activation, axonal injury, and phosphorylated tau immunoreactivity (Yu, Zhu et al. 2018, Verboon, Patel et al. 2021). However, the exact effects of rmTBI on brain functions and the underlying pathological mechanisms remain elusive.

The pathophysiology of rmTBI is characterized by complex changes in cerebral energy metabolism. Normally the brain uses glucose as the primary energy source; however, immediately after a traumatic injury, the metabolism in the brain switches to increased uptake and utilization of glucose relative to the rate of oxygen utilization. This altered metabolic state, called hyperglycosis, is characterized by uncoupling of glycolysis and oxidative phosphorylation and accumulation of lactic acid. This is followed by a prolonged period of cerebral glucose hypometabolism (Blanco, Prashant et al. 2016), during which ketone bodies are used as the main alternative fuel in the brain (Prins, Lee et al. 2004, Morris 2005, Thau-Zuchman, Svendsen et al. 2021). Cerebral ketone metabolism is an important compensatory metabolic pathway that bypasses the early glucose metabolic derangements after TBI.

Ketosis, or elevated plasma concentrations of ketone bodies, can be induced by a high-fat and low-carbohydrate ketogenic diet (KD) that induces a switch from glucose metabolism to fatty acid metabolism in the body (Prins, Fujima et al. 2005, Mychasiuk and Rho 2017, Salberg, Weerwardhena et al. 2019). The classic KD is an isocaloric, high-fat, very low-carbohydrate, and normal-protein diet initially designed to treat patients with refractory epilepsy, particularly children (Koppel and Swerdlow 2018, Ding, Lang et al. 2021). Due to the positive effects of KD on refractory epilepsy, its use has been extended to treat a wide variety of diseases, such as Parkinson disease, Alzheimer disease, stroke, and moderate-severe TBI (Rho and Stafstrom 2012, McDonald and Cervenka 2018). Furthermore, KD can improve neurological function and increase the expression of monocarboxylate transporter (MCT) in the rat after TBI, in an age-dependent manner (Appelberg, Hovda et al. 2009). Studies have shown that ketone bodies may mediate these benefits of KD. However, the exact mechanisms of beneficial effects of KD on TBI are not clear.

Gut microbiota plays an important role in the host physiology by impacting several metabolic and signaling pathways and neurological functions. The modulation of some of these pathways could be involved in the neuroprotection mediated by KD. It has been shown that KD alters the composition of gut microbiota in mice(Olson, Vuong et al. 2018), and ketosis in humans is associated with the change in gut microbiota composition (Klein, Newell et al. 2016). Several studies have revealed that the gut microbiota can metabolize amino acid tryptophan into indole and its derivatives, that can act as AHR ligands (Agus, Planchais et al. 2018).

AHR is a ligand-dependent transcription factor that regulates a diverse spectrum of cellular functions by regulating gene expression in a ligand- and cell-type-specific manner and has roles in regulating immunity, stem cell maintenance, and cellular differentiation(Chen, Chang et al. 2019). The research on dietary tryptophan derived AHR ligands has identified novel interactions between the gut microbiome and CNS inflammation.

L. reuteri is found as a gut symbiont in a number of mammalian species and has been described to participate in the transformation of dietary tryptophan into AHR agonists (Zelante, Iannitti et al. 2013). Interestingly, the abundance of *L. reuteri* is substantially altered in response to the KD (Olson, Vuong et al. 2018). *L. reuteri* can use tryptophan as an energy source, producing the AHR agonist 3-IAA as a metabolic product (Zelante, Iannitti et al. 2013). The microbial metabolites of tryptophan cross the blood–brain barrier and play a role in the inflammatory processes of the central nervous system by affecting AHR-driven mechanisms in microglia (Rothhammer, Mascanfroni et al. 2016). The latest research has also revealed that microglial AHR exerts both pro-inflammatory and anti-inflammatory effects in lipopolysaccharide-activated primary cultures of microglia, depending on the availability of exogenous AHR ligands (Lee, Lin et al. 2015). Therefore, the indole/AHR signaling pathway may play an important bridging role between the gut microbiota and microgliosis induced by rmTBI.

Microglial activation is one of the pathological changes occurring after rmTBI, and the mechanism of the regulatory effect of KD on microglial activation remains unknown. Among the variety of receptors

involved in the signaling leading to microglial activation, an important contributor is TLR4, which is mainly expressed on microglia. It has been reported that microglial pro-inflammatory function is activated by MyD88-dependent TLR4 signaling pathway after moderate-severe TBI (Zhang, Dong et al. 2018). Therefore, we hypothesized that KD would inhibit microglial activation after rmTBI by modulating the MyD88-dependent TLR4 signaling pathway.

In this study, we evaluated the therapeutic potential of KD on rmTBI in adolescent mice and explored the underlying mechanisms of its anti-neuroinflammation effects.

Materials And Methods

Animals and Experimental Design

All procedures involving animals in this study were approved by the Animal Care and Experimental Committee of the School of Medicine of Shanghai Jiao Tong University (permit number: RJ2021-0203). Specific pathogen-free (SPF), 3-4-week-old adolescent male C57BL/6 mice (10-12g) were used for the study. Mice were randomly divided into three groups after sample size estimation: sham group fed with the standard diet (SCG), rmTBI group fed with the standard diet (TCG), and rmTBI group fed with KD (TKG). Mice were housed in individual cages in a temperature and humidity-controlled animal facility with a 12-h light/dark cycle. Mice were kept in the animal facility for at least 7 days before surgery, and they were given free access to food and water during this period.

The sample size was not predetermined by a statistical method, but our sample sizes are similar to those generally used in the field. Furthermore, sample sizes for mouse experiments were sufficient for normality, variance homogeneity and statistical analyses. Randomization and blinding (the experimenter being blind to treatment group) were undertaken in all animal experiments. Experimenter blinding was sufficient to control for selection bias.

Repetitive Mild Traumatic Brain Injury Mouse Model

Mice were subjected to deep anesthesia with 2% isoflurane (RWD Life Science Co., Ltd, R510-22, Shenzhen, China) and were placed in a stereotaxic frame in the prone position. After shaving the head, an incision was made along the midline of the scalp, and a self-made concave metal disc was adhered to the head. Controlled cortical impact (CCI) injury was induced using a PinPoint^{TM} PCI3000 Precision Control Impactor^{TM} (Hatteras Instruments, Cary, North Carolina, USA) with the following settings: a 2.5 mm impactor tip with a speed of 1.0 m/s, a depth of 1.5 mm, and a dwell time of 100 ms. Control group mice were anesthetized only. After the injury, the scalp was closed with sutures. Repetitive injuries were induced for a total of 7 times within a 24-h interval. Mice were allowed to recover on a warm carpet (37°C) until fully awake and active and then returned to their cages.

Diet Interventions

Mice in each group were fed with either the standard diet (Xie Tong Biotechnology Co., Ltd, XTKDCON, Jiangsu, China) or KD (Xie Tong Biotechnology Co., Ltd, XTKD01, Jiangsu, China). The standard diet contained 10% protein, 80% carbohydrates, and 10% fat as (% kcal), and KD contained 10% protein and 90% fat (% kcal) as macronutrients. The caloric value of the standard diet and KD were 3.8 kcal/g and 6.7 kcal/g, respectively. In both the standard diet and KD, fat was derived from soybean oil and cocoa butter. Micronutrient content, fiber, and preservatives were matched on a per calorie basis. During experiments, mice had free access to the diets, which were placed in the food well of the cage-top wire lid. The composition of the control diet and KD are shown in Supplementary Tables 3 and 4.

Beam Walking

The goal of beam walking task was for the mouse to remain upright while traversing an elevated tapered beam (100 cm long, suspended horizontally 1m above ground) from one end to the other to reach a safe, dark box. Animals were trained to walk on the beam before surgery to reinforce the goal of the task, and three trials were conducted per mouse, with one-minute breaks between the trials. Performance on the beam was quantified by measuring the time taken by the mouse to walk across the beam and the number of hind-leg foot slips that occurred during the task. The beam-walk balance test was performed on day 7 post-injury.

Y-maze Test

Spatial working memory was measured by the Y-maze test. A Y-maze is a horizontal maze with three arms (50 cm in length and 10 cm in width) and walls (20 cm in height). The arms are symmetrically inclined to each other at 120°. Animals were set free for spontaneous movement throughout the Y-maze by placing them at the center of the maze. The mice typically like to explore a new arm of the maze, rather than returning to the one previously explored. An alternation sequence is the one when a mouse enters all three arms in a sequence without entering a single-arm twice in a row. A wrong alternation is when a mouse enters an arm two times in a row (Dowling and Allen 2018). The following equation was used to determine the percentage of the wrong alternations:

$$\%Wrongalteration = \frac{\text{Numberofwrongalterations}}{\text{Totalarmentries} - 2} \times 100\%$$

Tissue Preparation for Light Microscopy

At 7d after rmTBI, mice were subjected to deep anesthesia with 2% isoflurane and perfused transcardially with 4% paraformaldehyde (Beyotime Biotechnology Co., Ltd, P-0099, Shanghai, China). The brains were removed, further fixed at 4°C overnight in 4% paraformaldehyde, and then immersed in 30% sucrose/phosphate-buffered saline (PBS) (Beyotime Biotechnology Co., Ltd, C0221A, Shanghai, China) at 4°C overnight. Specimens were mounted in the optimal cutting temperature compound (OCT) (Sakura Finetek Co., Ltd, 4538, Japan). Serial sections were obtained using a cryostat and stained with toluidine blue for 30 min; two to three drops of glacial acetic acid were then added. Once the nucleus and the granulation were clearly visible, the specimens were mounted in Permount or Histoclad. Sections were cut in a microtome and adhered to glass slides with polylysine (all purchased from Beyotime Biotechnology Co., Ltd, C0105M, Shanghai, China). Images of the injured cortex and ipsilateral hippocampus were

captured at ×100 by using a light microscope (Nikon Labophot; Nikon USA, Melville, NY). There were three mice in each of the three groups. The cato

Beta-hydroxybutyrate (β-HB) and Glucose Analysis in Plasma

Blood samples were collected (n=10/group) through intracardiac sampling, plasma was prepared by centrifugation (12,000 ×g for 5min), and samples were divided into aliquots. A blood ketone and glucose monitoring system (FreeStyle Optium Neo, Abbott, NJ, USA) was used to measure blood ketone and glucose levels according to the manufacturer's instructions.

Silver Staining

Formalin-fixed OCT-embedded sections (40-µm-thick) were subjected to silver stain analysis to determine axonal damage. Silver staining was performed by using the FD NeuroSilver Kit II (FD NeuroTechnologies, PK301, Ellicott City, MD) according to the manufacturer's instructions but with some modifications. Densitometric analysis of silver staining was performed on 3 sections per mouse for corpus callosum. Images of the corpus callosum were captured at x200 by using a light microscope (Nikon Labophot; Nikon USA, Melville, NY) and were converted to grayscale with background subtraction. ImageJ software (NIH, Bethesda, MD) was used to quantify the staining on these digitized images (Winston, Noël et al. 2016). Silver staining was expressed in arbitrary units, ranging from 0 (minimum) to 255 (maximum) (Shitaka, Tran et al. 2011). There were three mice in each of the three groups.

In vivo Longitudinal Magnetic Resonance Imaging

In *vivo* MRI studies were performed on a 7-Telsa Bruker Biospec 70/20 USR spectrometer (Bruker BioSpin Corporation, Billerica, Massachusetts, USA) 7 days after the induction of rmTBI. Animals were placed onto a cradle with a stereotaxic head holder. Anesthesia was induced with 2% isoflurane via (1:1) N2O/O2 gas through a nose cone. Body temperature was maintained at 37.0°C using warm air, monitored, and controlled via a rectal temperature probe (CWE model TC-1000, Ardmore, Pennsylvania, USA). Conventional MR scanning sequence included T2WI and diffusion tensor imaging (DTI).

A whole brain anatomical T2-weighted scan using a Rapid Acquisition with Refocused Echoes (RARE) sequence was performed with the following parameters: TR = 5500 ms, TE = 37 ms, RARE factor = 8, FOV = 2.5×2.5 cm, in plane resolution = 109×109 µm, 600 µm slice thickness, 45 slices, and 12 min acquisition time. The diffusion images were acquired with a spin-echo and echo-planar imaging (EPI) sequence between the olfactory bulb and the cerebellum.

The diffusion tensor images were obtained for fractional anisotropy (FA) and mean diffusivity (MD) using a weighted linear least squares method (Winston, Noël et al. 2016). Finally, a region-of-interest (ROI) analysis was performed in the corpus callosum using the RadiAnt DICOM Viewer.

Immunohistochemical Staining

Formalin-fixed OCT-embedded frozen sections (40 μm thick) were permeabilized with 0.3% Triton X-100 (Beyotime Biotechnology Co., Ltd, ST797, Shanghai, China) in PBS, followed by blocking for 4 h in 0.3% Triton X-100 with 10% donkey serum (Beyotime Biotechnology Co., Ltd, A7039, Shanghai, China). The sections were incubated in the primary antibody diluted in 0.3% Triton X-100 with 10% donkey serum for 48 h at 4°C. After primary antibody incubation, the sections were washed in PBS and incubated in the secondary antibody diluted in 0.3% Triton X-100 with 10% donkey serum for 4h at room temperature (RT). Sections were washed three times in PBS and incubated in Hoechst 33342 (1:2,000; Thermo Fisher) for 15 min at RT for nuclear counterstaining. The sections were then mounted on microscope slides, sealed with clear nail polish, and stored at 4°C for preservation. The negative control sections were incubated with only secondary antibodies. There were six mice in each of the three groups. The antibody information is listed in Supplementary Tables 1 and 2.

In our study, omission of the primary antibody and incubation of the sections only with secondary antibodies was used to confirm the specificity of the different secondary antibodies.

Immunofluorescence Microscopy Analysis

In order to assess microglial infiltration and astrogliosis, at least 6 selected microscope fields in hippocampus were observed in each group (×200 magnifications; Zeiss LSM880; Zeiss, Germany), and microglia or astrocytes present in these fields were statistically analyzed. Furthermore, to observe the cellular localization and expression of AHR and RelB in microglia, randomly selected microscope fields were observed in each group (×400 magnifications; Zeiss LSM880; Zeiss, Germany). The negative control sections were observed in the same conditions. There were six mice in each of the three groups.

Western Blot Analysis

The hippocampus was harvested on day 7 after induction of rmTBI. The frozen brain samples were mechanically lysed in 20 mM tris (hydroxymethyl) aminomethane (Tris, pH 7.6), containing 0.2% sodium dodecyl sulfate (SDS), 1% Triton X-100, 1% deoxycholate, 1mM phenylmethylsulphonyl fluoride, and 0.11 IU/mL aprotinin (all purchased from Sigma–Aldrich, Inc., St. Louis, MO, USA). The lysates were centrifuged at 12,000 ×g for 15 min at 4°C and the supernatants were collected. The protein concentrations in the supernatants were estimated by the Bradford method.

The proteins (20 μg/lane) were separated on 12% SDS polyacrylamide gels and electro-transferred onto a polyvinylidene difluoride membrane (Bio-Rad Lab, Hercules, CA). The membrane was blocked with 5% skim milk (Beyotime Biotechnology Co., Ltd, P0216, Shanghai, China) (w/v) in Tris-buffered saline with 0.1% Tween-20 (TBST) (Beyotime Biotechnology Co., Ltd, ST825, Shanghai, China) for 1h at room temperature and incubated with primary antibodies diluted in TBST with for 24 h. After the membrane had been washed three times in TBST, 15 min each time, it was incubated with the appropriate horseradish peroxidase-conjugated secondary antibody diluted in TBST for 1h. The cross-reactive protein bands were visualized by enhanced chemiluminescence Western blot detection reagents (Millipore, Burlington, MA), and the results were quantified by Quantity One Software (Bio Rad, Hercules, CA, USA).

The band densities were calculated as ratios of TLR4 and MyD88/β-tubulin in the lanes. There were six mice in each of the three groups. The antibody information is listed in Supplementary Tables 1 and 2.

Enzyme-linked Immunosorbent Assay (ELISA) Analysis of Tumor Necrosis Factor (TNF), Interleukin-1 β (IL-1β), Chemokine (C-X-C motif) ligand 1 (CXCL1), Interferon Regulatory Factor 3 (IRF-3), and Indole-3-acetic (3-IAA)

On day 7 after rmTBI induction, mice were subjected to deep anesthesia by using 2% isoflurane. The brains were quickly removed by dissection and kept over ice in the physiologic salt solution. The hippocampus specimens were separated, cut into small pieces, dispersed by repeated aspiration into a pipette tip, and suspended in 1mL of physiologic salt solution with protease inhibitor (Beyotime Biotechnology Co., Ltd, P1006, Shanghai, China) in a test tube. Blood was collected by cardiac puncture, and the plasma was obtained by centrifugation (12,000 ×g for 5 min). The colon was washed and flushed with PBS to remove lumenal contents. Tissue samples were sonicated on ice in 10s intervals at 20 mV in RIPA lysis buffer (Beyotime Biotechnology Co., Ltd, P0013B, Shanghai, China), and the homogenates were centrifuged at 7500 rpm for 20 min. The supernatants were used for measuring the concentrations of cytokines and chemokines with commercial ELISA kits by following the manufacturer's instructions.

TNF (#JL10484), IL-1β (#JL18442), CCL1 (#JL42145), and IRF3 ELISA (#JL20345) kits were purchased from Jiang Lai Biotechnology Co., Ltd. (Shanghai, China). Quantification of 3-IAA in mouse was performed using an ELISA kit (abx150354, Abbexa Ltd., Sugar Land, TX, USA) according to a previously described method (Constante, De Palma et al. 2021). There were six mice in each of the three groups.

DNA Extraction from Fecal Samples

Bacterial DNA from frozen fecal samples was extracted using a QIAamp DNA stool mini kit (Qiagen, Hilden, 51504, Germany) according to the manufacturer's instructions and stored at −20°C until use. Nanodrop One spectrophotometer (Thermo Scientific, Wilmington, DE, USA) was used to quantify the DNA concentration, and the quality of the extracted DNA was estimated by the ratio of absorbance at 260 and 280 nm.

Standard Curve for qPCR

The standard curve was constructed by plotting the threshold cycles (Ct) values against the log input extracted DNA from respective dilutions of bacterial suspension of a reference strain of *L. reuteri* (Jomehzadeh, Javaherizadeh et al. 2020). Briefly, *L. reuteri* reference strain was grown in 5mL of MRS broth (Huaikai microbial Co., Ltd, 027312, Guangdong, China) to an OD 600nm of 0.6 on a Nanodrop One spectrophotometer (Thermo Scientific, Wilmington, DE, USA) and serially diluted to a final concentration range of 10^1–10^7 CFU mL^{-1}. A 100µL of each dilution was plated on MRS agar and incubated under the microaerophilic condition for 48h at 37°C. Colonies were then enumerated and used for colony-forming unit extrapolation (CFU per milliliter). All experiments were performed at least in triplicate, and the average titer (CFU mL^{-1}) of three replicates was determined. Community DNA from feces was extracted using a

QIAamp DNA stool mini kit (Qiagen, Hilden, 51504, Germany) as described above. By comparing the Ct values acquired to the standard curve, the number of cells of *L. reuteri* in the fecal samples were determined.

Quantitative Real-Time PCR

As previously described, Real-time quantitative PCR was performed using *L. reuteri* specific primers (Jomehzadeh, Javaherizadeh et al. 2020). Total bacterial DNA was applied as a template for qPCR. The qPCR reaction volume of 20 µL contained 2 µL of 50 ng/µL of DNA template, each of forward and reverse primer in a volume of 0.4 µL, 10 µL of SYBR Advantage Premix, and nuclease-free water added to obtain the final volume of 20 µL (all purchased from Beyotime Biotechnology Co., Ltd, D7265, Shanghai, China). Initial denaturation at 95°C for 30 s were followed by 40 cycles at 95°C for 10 s, annealing at 60°C for 30 s and extension at 70°C for 15 s, and final elongation at 72°C for 5 min. All experiments were performed in triplicates. There were four mice in each of the three groups. The following *L. reuteri* specific primer pair was used: Lreu-1: 5’- CAGACAATCTTTGATTGTTTAG -3’; Lreu-4: 5’- GCTTGTTGGTTTGGGCTCTTC -3’.

Statistical Analysis

All data are presented as mean ± standard deviation (SD). Statistical analysis was performed using GraphPad Prism 9 (GraphPad Software, San Diego, USA). All data were subjected to one-way ANOVA followed by Tukey’s test. Statistical significance was inferred at $P < 0.05$. Normality was checked by Shapiro-Wilk test, and homogeneity of variance was checked by Brown-Forsythe test in multiple groups. The results showed that the variance was similar. The results of the tests for normality and variance homogeneity are shown in Supplementary Tables 5 and 6.

Results

A Stable Repetitive Mild Traumatic Brain Injury Mouse Model Was Established.

The rmTBI mouse model was induced with the CCI device. All mice were then subjected to dietary interventions. One week later, all mice were subjected to behavioral tests and experimental analysis (Fig. 1A). The hematoxylin & eosin (HE) staining of neurons and T2 weighted imaging (T2WI) were performed in our study. The general view and HE staining of the brains showed that rmTBI did not induce acute brain damage, including contusion and hemorrhage (Fig. 1B). Furthermore, no acute brain damage was observed in the brains of SCG and TCG mice in T2WI, suggesting that the impacts did not induce a moderate or severe brain injury (Fig. 1C).

KD Elevated Serum β-HB and Decreased Serum Glucose After rmTBI.

β-HB and glucose levels were measured in serum with blood ketone and glucose monitoring system. It is well-established that KD is associated with an induction of higher ketone levels and low glucose levels. Significantly increased serum β-HB level and decreased serum glucose level were detected in TKG mice, compared with the SCG and TCG mice (Fig. 2A, B). Moreover, significantly more body weight loss was

observed over the course of the experiment in mice in TKG, compared with those in SCG or TCG (Fig. 2C). These results indicate the presence of ketotic state in mice fed with KD.

rmTBI Caused Neurobehavioral Dysfunction, Which Was Ameliorated by KD.

The neurobehavioral assessments were performed on 7th day post-injury. The balance and motor coordination of mice were assessed using the beam walk test. Average crossing time and hind-leg foot slips significantly increased in TCG mice, as compared with SCG mice. Moreover, KD decreased average crossing time and hind-leg foot slips in TKG mice compared with TCG mice (Fig. 3A, B). Moreover, the memory dysfunction as assessed by the Y-maze test indicated that rmTBI caused significant impairment of spatial working memory in TCG mice, compared with that in SCG mice; TKG (0.28±0.07, $P < 0.05$) mice showed significantly improved memory performance in the Y maze test (Fig. 3C). These observations indicate that KD treatment could ameliorate neurobehavioral dysfunction caused due to rmTBI.

rmTBI Caused Axonal Injury, Which Was Alleviated by KD.

Silver staining revealed abnormalities of white matter in the brains of TCG and TKG mice. The density of silver staining in the corpus callosum of TCG mice on 7th day post-injury showed significant axonal damage compared with that in SCG mice. However, there was a significant reduction of corpus callosum silver staining density in TKG mice (Fig. 4A, C).

FA and MD are the most commonly used DTI-derived metrics, which are believed to reflect overall white matter health. On 7th day after rmTBI, TCG mice showed increased FA and MD values in the corpus callosum compared with those in SCG. Meanwhile, TKG mice showed decreased FA and MD values, as compared with TCG mice (Fig. 4B, D and E). Thus, axonal damage on 7th day after rmTBI, was significantly alleviated by KD.

rmTBI Led to Microglial Activation and Astrogliosis, Which Were Inhibited by KD.

rmTBI is followed by microglial activation and other neuroinflammatory responses. Change in microglial activation was evaluated by the number of Iba-1 positive cells in hippocampus by immunohistochemical staining. We found that the number of Iba-1 positive cells was dramatically increased in TCG mice, as compared with SCG mice. Meanwhile, the number of Iba-1 positive cells were decreased in TKG mice, as compared with TCG mice (Fig. 5A, C).

Immunohistochemical staining of astrocyte marker-glial fibrillary acidic protein (GFAP) was used to evaluate astrogliosis in hippocampus. Mice in TCG had significantly increased number of GFAP-positive cells, as compared with SCG mice, and mice in TKG had fewer GFAP-positive cells, as compared with TCG mice (Fig. 5B, D). These observations indicate that rmTBI caused microglial activation and astrogliosis, which were suppressed by KD.

rmTBI Activated L. reuteri **Mediated Indole/AHR Signaling Pathway, Which Was Inhibited by KD.**

Standard curve obtained by plotting the average Ct values against the estimated $\log_{10}$ CFU for *L. reuteri* is shown in Figure 6A. The amounts of *L. reuteri* (Log_{10} CFU/gram of feces) were determined in mice feces with qRT-PCR. The results showed that the amount of *L. reuteri* (Log_{10} CFU/gram of feces) in TCG mice was markedly increased compared with that in SCG mice. KD reduced the amount of *L. reuteri* in TKG mice, compared with that in TCG mice (Fig. 6B).

To determine the role of indole/AHR pathway in microglial activation, we measured the levels of 3-IAA with ELISA, a potential endogenous AHR ligands in serum, large intestines, and brains in mice. The results showed that the levels of 3-IAA levels in TCG mice were markedly increased compared with those in SCG mice. Moreover, KD decreased the levels of 3-IAA in TKG mice (Fig. 6C-E). There were no significant differences in the levels of 3-IAA between SCG and TKG mice.

Mechanistically, AHR can modulate microglial activation via competitive binding with RelB. Therefore, we further investigated the expression and nuclear localization of AHR and RelB in microglia on 7th day after rmTBI, using immunofluorescent staining of AHR/RelB and microglial marker Iba-1 (Vogel and Matsumura 2009, Chen, Chang et al. 2019). Immunohistochemical analysis revealed that TCG mice showed a marked increase in the expression of AHR/RelB and co-localization in the nucleus of Iba1 positive microglia, as compared with SCG mice. In TKG mice, compared with TCG mice, the AHR/RelB co-localization was more pronounced in the microglial cytosol than in the nucleus (Fig. 7A). The negative control images have been added to supplementary materials (Supplementary Figure 1).

CCL1 and IRF3 are involved in the microglial activation after rmTBI. Thus, the levels of CCL1 and IRF3 in hippocampus were determined with ELISA. The results showed that the expressions of CCL1 and IRF3 in TCG mice were markedly increased in TCG mice compared with those in SCG mice. KD attenuated the expressions of CCL1 and IRF3 in TKG mice (Fig. 7B, C). Collectively, these results suggest that *L. reuteri* mediated indole/AHR signaling pathway might participate in the pathological development of rmTBI by modulating microglial inflammatory activation and KD played an important role in suppressing *L. reuteri* mediated indole/AHR signaling pathway.

rmTBI Activated the TLR4/MyD88 Mediated NF-κB Pathway, Which Was Inhibited by KD.

Expression levels of TLR4 and MyD88 in microglia were measured with Western blotting. Increased levels of TLR4 and MyD88 were observed in the hippocampus of mice in TCG on 7th day post-rmTBI, compared with those in SCG mice. Moreover, KD decreased levels of TLR4 and MyD88 in TKG mice (Fig. 8A-C and Supplementary materials).

TNF and IL-1β are involved in neuroinflammatory responses after rmTBI. Hence, the levels of TNF and IL-1β in hippocampus were determined with ELISA. Our results revealed that the expression levels of TNF and IL-1β in TCG mice were markedly increased compared with those in SCG mice. KD attenuated the expressions of TNF and IL-1β in TKG mice, compared with those in TCG mice (Fig. 8D, E). Taken together, these findings suggested that rmTBI activated the TLR4/MyD88 mediated NF-κB pathway, which was inhibited by KD.

Discussion

It was found that rmTBI induced by CCI caused axonal damage, microglial activation and astrogliosis, and impaired neurological functions. KD given immediately post rmTBI in adolescent mice significantly increased the blood β-HB levels and led to functional neurological benefits. KD, compared with control diet, inhibited the microgliosis and pro-inflammatory activation after rmTBI. Furthermore, rmTBI also activated TLR4/MyD88 mediated NF-κB pathway and 3-IAA mediated AHR pathway, which were attenuated by KD.

rmTBI triggers axonal injury, which is associated with post-traumatic neuro-behavioral impairment. Silver staining and DTI are two reliable approaches for the estimation of axonal damage after rmTBI. Several studies have confirmed that acute axonal injury in various white matter regions in rmTBI is indicated by argyrophilic structures and significant silver uptake compared to sham (Winston, Noël et al. 2016). Of all regions, the corpus callosum may have the most prominent and persistent course of silver staining abnormalities at 7 days (Hylin, Orsi et al. 2013). FA and MD are the most commonly used DTI-derived metrics, which are believed to reflect overall white matter health, maturation, and organization (Hofstetter and Assaf 2017). In this study, results of silver staining and DTI showed significant axonal injury 7 days post-rmTBI. The increased intensity of silver staining in the injured mice correlated with their impaired motor coordination, as assessed by the beam walking test. We found that KD could ameliorate axonal damage and improve motor coordination in mice with rmTBI.

KD protects myelinated axons by increasing myelination that could improve axonal energy support (Stumpf, Berghoff et al. 2019). TBI-induced changes in cerebral glucose metabolism occur as a series of neurochemical events (Prins and Matsumoto 2016). When cerebral metabolism of glucose is compromised following brain injury, ketones can fulfill the energy requirements of the brain cells. Classical KD, with high-fat and low-carbohydrate content, can increase ketone levels and act as alternative substrates for all cell types. These ketone bodies stimulate mitochondrial metabolism and increase its metabolic efficiency, reduce the production of reactive oxygen species, and supply up to 70% of the energy required for brain function (Thau-Zuchman, Svendsen et al. 2021). Therefore, KD may be beneficial for the treatment for axonal damage following rmTBI.

Studies on KD have shown that a fat-rich and carbohydrate-poor diet can inhibit microglial activation after moderate-severe TBI (Thau-Zuchman, Svendsen et al. 2021). Studies examining the mechanisms of therapeutic effects of KD on rmTBI are lacking. In this study, we have demonstrated that rmTBI caused reactive microgliosis, which was ameliorated by KD. In addition to reducing the number of activated microglia, KD may also directly affect the microglial pro-inflammatory function(Guan, Huang et al. 2020). This negative regulatory effect of KD may play an important role in reducing neuroinflammation mediated by microglia after rmTBI. Therefore, further explorations were conducted to elucidate underlying mechanisms of KD-regulated microglial activation.

Since inflammatory damage is the key pathophysiological feature of rmTBI, we chose microglial activation as the focus in our research to study the mechanisms underlying the beneficial effects of KD

on rmTBI. Multiple molecular pathways, such as STAT and nuclear factor-κB (NF-κB) are involved in the regulation of microglial activation (Qin, Yeh et al. 2012, Kobayashi, Imagama et al. 2013, Tanaka, Murakami et al. 2015). Previous studies have reported that moderate-severe TBI activated the TLR4/MyD88 mediated NF-κB pathway in microglial cells (Zhang, Dong et al. 2018). Our results show that KD could suppress the expression of TLR4 and MyD88 and negatively modulate the level of the inflammatory cytokines TNF and IL-1β 7 days after rmTBI. However, the mechanism by which KD regulates the TLR4/MyD88 mediated NF-κB pathway after rmTBI is not clear.

AHR could be activated by numerous exogenous compounds. Indole and its derivates such as 3-IAA and indole-3-propionic acid (3-IPA) have been identified as high-affinity endogenous ligands to the AHR (Gao, Mu et al. 2020). Gut microbiota can impact levels of various neuroactive molecules in the peripheral nervous system and the brain (Vuong, Yano et al. 2017). Tryptophan, an essential amino acid in the diet, can be converted to 3-IAA by some bacteria of genus *Lactobacillus* and *Bifidobacterium* through aromatic amino acid aminotransferase and indole lactic acid dehydrogenase–dependent pathways (Cervantes-Barragan, Chai et al. 2017, Gao, Mu et al. 2020). Moreover, it has been reported that KD altered the gut microbiota and significantly decreased *L. reuteri* in mice fed with KD (Olson, Vuong et al. 2018). However, whether *L. reuteri* mediated indole/AHR signaling pathway is involved in the regulation of KD on microglial activation after rmTBI was unclear.

Mechanistically, activated AHR translocates into the nucleus, interacts with RelB, and occupies RelB/AHR-response elements (RelB/AHRE) of promoters, resulting in activation of downstream target genes, like CCL1, IRF3 (Vogel and Matsumura 2009). It has been reported that AHR signaling potentially mediates post-stroke gliosis and ischemic brain injuries (Chen, Chang et al. 2019). In this study, we have shown that *L. reuteri*-produced tryptophan metabolite, 3-IAA, is associated with microglial activation in the brain. Our study found that there were reduced co-localization of AHR/RelB in the microglial nucleus and lower level of CCL1 and IRF3 in mice fed with KD, post-rmTBI. Thus, *L. reuteri* may participate the modulation of KD on microglial activation after rmTBI through indole/AHR signaling.

Conclusion

Axonal damage, microglial activation and astrogliosis induced by rmTBI could be ameliorated in adolescent mice by giving KD immediately after rmTBI. KD significantly increased blood β-HB levels and provided functional neurological benefits. *L. reuteri* mediated indole/AHR and downregulated TLR4/MyD88 mediated NF-κB signaling pathways in microglia were inhibited after KD intervention, which indicated a suppressed neuroinflammation related to microglial activation. Our study provides insights into the potential mechanisms of beneficial effects of KD in rmTBI in adolescent mice.

Limitations

The exact mechanism by which KD affects the synthesis of indole compounds in the gut microbiota remains unclear. Inhibition of the indole/AHR pathway in microglial cells is the next logical step for

confirmation of the role of gut microbiota produced indole metabolites in mediating the inhibitory effect of KD on microglial activation. Several studies have reported age-related differences in the neuroprotection provided by KD and MCT expression after TBI (Appelberg, Hovda et al. 2009). We have chosen adolescent mice for this study, further studies are required to verify the beneficial effect of KD on adult mice with rmTBI.

Abbreviations

3-IAA: indole-3-acetic-acid; AHR: Aryl hydrocarbon receptor; β-HB: Beta-hydroxybutyrate; CXCL1: Chemokine (C-X-C motif) ligand 1; CCI: Controlled cortical impact; DTI: diffusion tensor imaging; ELISA: Enzyme-linked immunosorbent assay; FA: Fractional anisotropy; GFAP: Glial fibrillary acidic protein; HE: Hematoxylin and eosin; IL-1β: Interleukin β1; IRF-3: Interferon regulatory Factor 3; Iba-1: Ionized calcium-binding adapter molecule 1; KD: Ketogenic diet; MyD88: Myeloid differentiation primary response 88; MCT: monocarboxylate transporter; MD: mean diffusivity; NF-κB: Nuclear factor kappa light chain enhancer of activated B cells; OCT: Optimal cutting temperature compound; PBS: Phosphate-buffered saline; rmTBI: Repetitive mild traumatic brain injury; TLR4: Toll-like receptor 4; TNF: Tumor necrosis factor;

Declarations

Acknowledgments

We thank the entire the laboratory of Neurosurgery Department for supporting experimental space and technical services.

Author Contributions

DD, FZ and YJ designed the experiments. DD, FZ and SS performed and analyzed most experiments with the help of TL, MC, QL. DD and FZ were major contributors in writing this manuscript. FJ and XZ participated in the discussions and revised the manuscript. YJ supervised the entire project and was responsible for finalizing and submitting the manuscript. All authors read and approved the final manuscript.

Funding

This work was supported by grants from the National Natural Science Foundation of China (No. 82071359), the Shanghai Rising-Star Program (21QA1405600), the Natural Science Foundation of Shanghai (21ZR1439000) and Ren ji New Star Program (F. Jia).

Data Availability Statement

The original contributions presented in the study are included in the article. Further inquiries can be directed to the corresponding author.

Conflict of Interest

The authors declare that they have no competing interests.

Ethics Statement

Animal protocols were approved by the Animal Care and Experimental Committee of the School of Medicine of Shanghai Jiao Tong University.

References

1. Agus A et al (2018) Gut microbiota regulation of tryptophan metabolism in health and disease. Cell Host Microbe 23(6):716–724. DOI: 10.1016/j.chom.2018.05.003
2. Appelberg KS et al (2009) The effects of a ketogenic diet on behavioral outcome after controlled cortical impact injury in the juvenile and adult rat. J Neurotrauma 26(4):497–506. DOI: 10.1089/neu.2008.0664
3. Blanco MMB et al (2016) Cerebral metabolism and the role of glucose control in acute traumatic brain injury. Neurosurgery Clinics 27(4):453–463. DOI: 10.1016/j.nec.2016.05.003
4. Cervantes-Barragan L et al (2017) Lactobacillus reuteri induces gut intraepithelial CD4+ CD8αα + T cells. Science 357(6353):806–810. DOI: 10.1126/science.aah5825
5. Chen W-C et al (2019) Aryl hydrocarbon receptor modulates stroke-induced astrogliosis and neurogenesis in the adult mouse brain. J Neuroinflamm 16(1):1–13. DOI: 10.1186/s12974-019-1572-7
6. Constante M et al (2021) Saccharomyces boulardii CNCM I-745 modulates the microbiota–gut–brain axis in a humanized mouse model of Irritable Bowel Syndrome. Neurogastroenterol Motil 33(3):e13985. DOI: 10.1111/nmo.13985
7. Ding M et al (2021) Microbiota–Gut–Brain Axis and Epilepsy: A Review on Mechanisms and Potential Therapeutics. Frontiers in Immunology 4131.. DOI: 10.3389/fimmu.2021.742449
8. Dowling C, Allen NJ (2018) Mice lacking glypican 4 display juvenile hyperactivity and adult social interaction deficits. Brain Plasticity 4(2):197–209. DOI: 10.3233/BPL-180079
9. Gao K et al (2020) Tryptophan metabolism: a link between the gut microbiota and brain. Advances in Nutrition 11(3):709–723. DOI: 10.1093/advances/nmz127
10. Guan Y-F et al (2020) Anti-depression effects of ketogenic diet are mediated via the restoration of microglial activation and neuronal excitability in the lateral habenula. Brain Behav Immun 88:748–762. DOI: 10.1016/j.bbi.2020.05.032
11. Hofstetter S, Assaf Y (2017) The rapid development of structural plasticity through short water maze training: A DTI study. NeuroImage 155:202–208. DOI: 10.1016/j.neuroimage.2017.04.056
12. Hylin MJ et al (2013) Behavioral and histopathological alterations resulting from mild fluid percussion injury. J Neurotrauma 30(9):702–715. DOI: 10.1089/neu.2012.2630

13. Jomehzadeh N et al (2020) Quantification of intestinal lactobacillus species in children with functional constipation by quantitative real-time PCR. Clin Exp Gastroenterol 13:141. DOI: 10.2147/CEG.S250755
14. Klein MS et al (2016) Metabolomic modeling to monitor host responsiveness to gut microbiota manipulation in the BTBRT+ tf/j mouse. J Proteome Res 15(4):1143–1150. DOI: 10.1021/acs.jproteome.5b01025
15. Kobayashi K et al (2013) Minocycline selectively inhibits M1 polarization of microglia. Cell Death Dis 4(3):e525–e525. DOI: 10.1038/cddis.2013.54
16. Koppel SJ, Swerdlow RH (2018) Neuroketotherapeutics: a modern review of a century-old therapy. Neurochem Int 117:114–125. DOI: 10.1016/j.neuint.2017.05.019
17. Lee YH et al (2015) Aryl hydrocarbon receptor mediates both proinflammatory and anti-inflammatory effects in lipopolysaccharide-activated microglia. Glia 63(7):1138–1154. DOI: 10.1002/glia.22805
18. Maas AI et al (2017) Traumatic brain injury: integrated approaches to improve prevention, clinical care, and research. Lancet Neurol 16(12):987–1048. DOI: 10.1016/S1474-4422(17)30371-X
19. McDonald TJ, Cervenka MC (2018) The expanding role of ketogenic diets in adult neurological disorders. Brain sciences 8(8):148. DOI: 10.3390/brainsci8080148
20. Morris A (2005) Cerebral ketone body metabolism. J Inherit Metab Dis 28(2):109–121. DOI: 10.1007/s10545-005-5518-0
21. Mychasiuk R, Rho JM (2017) Genetic modifications associated with ketogenic diet treatment in the BTBRT+ Tf/J mouse model of autism spectrum disorder. Autism Res 10(3):456–471. DOI: 10.1002/aur.1682
22. Olson CA et al (2018) The gut microbiota mediates the anti-seizure effects of the ketogenic diet. Cell 173(7):1728–1741. e1713 DOI: 10.1016/j.cell.2018.04.027
23. Prins M et al (2005) Age-dependent reduction of cortical contusion volume by ketones after traumatic brain injury. J Neurosci Res 82(3):413–420. DOI: 10.1002/jnr.20633
24. Prins M et al (2004) Increased cerebral uptake and oxidation of exogenous βHB improves ATP following traumatic brain injury in adult rats. J Neurochem 90(3):666–672. DOI: 10.1111/j.1471-4159.2004.02542.x
25. Prins ML, Matsumoto J (2016) Metabolic response of pediatric traumatic brain injury. J Child Neurol 31(1):28–34. DOI: 10.1177/0883073814549244
26. Qin H et al (2012) Signal transducer and activator of transcription-3/suppressor of cytokine signaling-3 (STAT3/SOCS3) axis in myeloid cells regulates neuroinflammation. Proceedings of the National Academy of Sciences 109 (13): 5004-5009. DOI: 10.1073/pnas.1117218109
27. Rho JM, Stafstrom CE (2012) The ketogenic diet as a treatment paradigm for diverse neurological disorders. Front Pharmacol 3:59. DOI: 10.3389/fphar.2012.00059
28. Rothhammer V et al (2016) Type I interferons and microbial metabolites of tryptophan modulate astrocyte activity and central nervous system inflammation via the aryl hydrocarbon receptor. Nat

Med 22(6):586–597. DOI: 10.1038/nm.4106

29. Salberg S et al (2019) The behavioural and pathophysiological effects of the ketogenic diet on mild traumatic brain injury in adolescent rats. Behav Brain Res 376:112225. DOI: 10.1016/j.bbr.2019.112225
30. Shitaka Y et al (2011) Repetitive closed-skull traumatic brain injury in mice causes persistent multifocal axonal injury and microglial reactivity. Journal of Neuropathology & Experimental Neurology 70(7):551–567. DOI: 10.1097/NEN.0b013e31821f891f
31. Stumpf SK et al (2019) Ketogenic diet ameliorates axonal defects and promotes myelination in Pelizaeus–Merzbacher disease. Acta Neuropathol 138(1):147–161. DOI: 10.1007/s00401-019-01985-2
32. Tanaka T et al (2015) Interferon regulatory factor 7 participates in the M 1-like microglial polarization switch. Glia 63(4):595–610. DOI: 10.1002/glia.22770
33. Thau-Zuchman O et al (2021) A new ketogenic formulation improves functional outcome and reduces tissue loss following traumatic brain injury in adult mice. Theranostics 11(1):346. DOI: 10.7150/thno.48995
34. Verboon LN et al (2021) The immune system's role in the consequences of mild traumatic brain injury (concussion). Frontiers in Immunology 12 313.. DOI: 10.3389/fimmu.2021.620698
35. Vogel CF, Matsumura F (2009) A new cross-talk between the aryl hydrocarbon receptor and RelB, a member of the NF-κB family. Biochem Pharmacol 77(4):734–745. DOI: 10.1016/j.bcp.2008.09.036
36. Vuong HE et al (2017) The microbiome and host behavior. Annu Rev Neurosci 40:21–49. DOI: 10.1146/annurev-neuro-072116-031347
37. Winston CN et al (2016) Dendritic spine loss and chronic white matter inflammation in a mouse model of highly repetitive head trauma. Am J Pathol 186(3):552–567. DOI: 10.1016/j.ajpath.2015.11.006
38. Yu J et al (2018) Impact of nutrition on inflammation, tauopathy, and behavioral outcomes from chronic traumatic encephalopathy. J Neuroinflamm 15(1):1–16. DOI: 10.1186/s12974-018-1312-4
39. Zelante T et al (2013) Tryptophan catabolites from microbiota engage aryl hydrocarbon receptor and balance mucosal reactivity via interleukin-22. Immunity 39(2):372–385. DOI: 10.1016/j.immuni.2013.08.003
40. Zhang F et al (2018) Moderate hypothermia inhibits microglial activation after traumatic brain injury by modulating autophagy/apoptosis and the MyD88-dependent TLR4 signaling pathway. J Neuroinflamm 15(1):1–12. DOI: 10.1186/s12974-018-1315-1

Figures

Figure 1

A stable repetitive mild traumatic brain injury mouse model was established.

A Experimental design for rmTBI model and diet interventions. Mice received a sham surgery or repetitive mild impacts consecutively for 7 days, after which they were fed a standard diet or KD for 7 more days. The subsequent behavioral tests and molecular experiments were performed on day 7 post-injury.

B The general view and HE staining of the brains from SCG and TCG mice 7 days after rmTBI. No acute brain damage was observed on the brains of SCG and TCG mice.

C Representative T2WI of the brains from sham and rmTBI mice. rmTBI did not induce acute macroscopic brain damage, including contusion and hemorrhage.

Figure 2

KD elevated serum β-HB and decreased serum glucose after rmTBI.

A and B Levels of serum ß-HB and glucose in mice fed standard diet or KD for 7 days. Data in the bar graphs represent mean ± SD. Serum β-HB: n = 6, 13, 11; one-way ANOVA; $P = 0.8183$, $^{****}P < 0.0001$, $^{****}P < 0.0001$; $F_{2, 28} = 1.358$, $P = 0.2871$; serum glucose: n = 6; one-way ANOVA; $P = 0.7692$, $^{****}P < 0.0001$, $^{****}P < 0.0001$; $F_{2, 15} = 1.908$, $P = 0.1826$.

C Line graph showing the dynamic changes in body weight of mice in different groups. n=10/each group.

Figure 3

rmTBI caused functional impairments, which were ameliorated by KD.

A Time to beam walk; **B** Number of foot slips in the beam walk task. Both SCG and TKG mice showed marked improvement compared with the TCG mice. Data in the bar graphs represent mean ± SD. Average crossing time: n = 10; one-way ANOVA; $^{**}P = 0.0012$, $P = 0.5878$, $^{*}P = 0.0143$; $F_{2, 27} = 0.2959$, $P = 0.7462$; hind-leg foot slips: one-way ANOVA; $^{***}P = 0.0005$, $P = 0.3471$, $^{**}P = 0.0060$; $F_{2, 27} = 1.518$, $P = 0.2372$.

C Memory function assessment with the Y-maze test. A significant increase of wrong alteration was seen in TCG mice compared to those in SCG mice, and this was markedly reduced in TKG mice. Data in the bar graphs represent mean ± SD. N = 13, 10, 12; one-way ANOVA; $^{*}P = 0.0137$, $P = 0.8725$, $^{*}P = 0.0467$; $F_{2, 32} = 2.139$, $P = 0.1344$.

Figure 4

rmTBI caused axonal injury, which was alleviated by KD.

A Representative silver staining of the corpus callosum in different groups. Placement of the regions of interest in the corpus callosum (white box).

B Representative T2WI and DTI images of the corpus callosum in different groups. Placement of the regions of interest in the corpus callosum (yellow area).

C Analysis of intensity of silver staining in the corpus callosum from SCG, TCG, TKG mice. Data in the bar graphs represent mean ± SD. N = 6; one-way ANOVA; ****$P < 0.0001$, *$P = 0.0230$, **$P = 0.0066$; $F_{2, 15} = 0.4987$, $P = 0.6170$.

D Evaluation of FA in the corpus callosum from SCG, TCG, TKG mice. Data in the bar graphs represent mean ± SD. N = 6; one-way ANOVA; *$P = 0.0112$, $P = 0.9643$, *$P = 0.0186$; $F_{2, 15} = 0.6393$, $P = 0.5415$.

E Evaluation of MD in the corpus callosum from SCG, TCG, TKG mice. Data in the bar graphs represent mean ± SD. N = 6; one-way ANOVA; **$P = 0.0011$, $P = 0.3988$, *$P = 0.0153$; $F_{2, 15} = 0.4786$, $P = 0.6288$.

Figure 5

rmTBI led to microglial activation and astrogliosis, which were inhibited by KD.

A and B Representative immunohistochemical staining of Iba-1 or GFAP from hippocampus.

C and D Quantification of Iba-1 or GFAP positive cells in hippocampus. Data in the bar graphs represent mean ± SD. Iba-1: n = 6; one-way ANOVA; **$P = 0.0016$, $P = 0.7811$, ***$P = 0.0004$; $F_{2, 15} = 1.837$, $P = 0.1934$; GFAP: n = 6; one-way ANOVA; ***$P = 0.0002$, $P = 0.0717$, *$P = 0.0252$; $F_{2, 15} = 0.3737$, $P = 0.6944$.

Figure 6

KD downregulated microbial tryptophan metabolism by gut microbiota after rmTBI.

A Representative standard curve obtained by plotting the average C_t values against the estimated $\log_{10}$ CFU/PCR for *L. reuteri*.

B Quantity *of L. reuteri* in the feces of different groups. Data in the bar graphs represent mean ± SD. N = 6; one-way ANOVA; ****$P < 0.0001$, **$P = 0.0055$, ****$P < 0.0001$; $F_{2, 15} = 0.0225$, $P = 0.9778$.

C, D and E Concentration of 3-IAA in the large intestines, sera and brains, as determined by ELISA. Data in the bar graphs represent mean ± SD. 3-IAA in large intestines: n = 6; one-way ANOVA; ***$P = 0.0002$, $P =$

0.9938, ***P = 0.0002; $F_{2, 15}$ = 1.094, P = 0.3601; 3-IAA in serum: n = 6; one-way ANOVA; ***P = 0.0008, P = 0.9812, **P = 0.0011; $F_{2, 15}$ = 0.1263, P = 0.8823; 3-IAA in brains: n = 6; one-way ANOVA; *P = 0.0139, P = 0.2686, ***P = 0.0006; $F_{2, 15}$ = 3.351, P = 0.0626.

Figure 7

rmTBI activated the *L. reuteri* mediated indole/AHR signaling pathway, which was inhibited by KD.

A Representative confocal images of AHR/RelB colocalization in microglia from the hippocampus. Solid arrows indicate co-localization of AHR and RelB in the nucleus. Hollow arrows indicate co-localization of AHR and RelB in the cytosol.

B and C ELISA of CCL1 and IRF3 from hippocampus after rmTBI. Data in the bar graphs represent mean ± SD. CCL1: n = 6; one-way ANOVA; *P = 0.0122, P = 0.2096, ***P = 0.0004; $F_{2, 15}$ = 0.2224, P = 0.8032; IRF3: n = 6; one-way ANOVA; *P = 0.0163, P = 0.9715, *P = 0.0103; $F_{2, 15}$ = 0.0940, P = 0.9108.

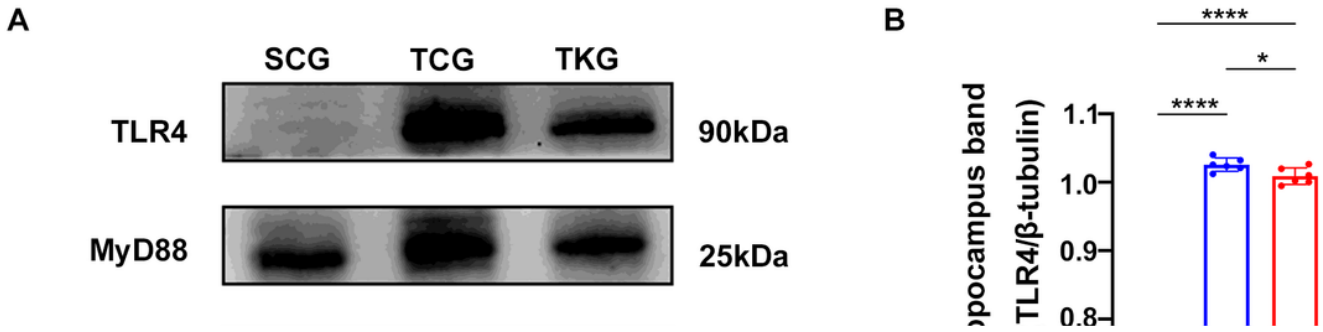

Figure 8

rmTBI activated the TLR4/MyD88 mediated NF-κB pathway, which was inhibited by KD.

A Representative western blotting of TLR4 and MyD88 from hippocampus.

B and C Analysis the expression of TLR4 and MyD88 from hippocampus, with β-tubulin as the loading control. TLR4: n = 6; one-way ANOVA; ****$P < 0.0001$, ****$P < 0.0001$, *$P = 0.0416$; $F_{2, 15} = 0.3662$, $P = 0.6994$; MyD88: n = 6; one-way ANOVA; **$P = 0.0066$, $P = 0.8670$, *$P = 0.0183$; $F_{2, 15} = 0.0779$, $P = 0.9254$.

D and E Concentrations of TNF and IL-1β in hippocampus after rmTBI, as determined by ELISA. Data in the bar graphs represent mean ± SD. TNF: n = 6; one-way ANOVA; *$P = 0.0131$, $P = 0.9113$, *$P = 0.0294$; $F_{2, 15} = 0.0117$, $P = 0.9884$; IL-1β: n = 6; one-way ANOVA; *$P = 0.0162$, $P = 0.9141$, *$P = 0.0115$; $F_{2, 15} = 1.858$, $P = 0.1901$.

Supplementary Files

This is a list of supplementary files associated with this preprint. Click to download.

- GraphicalAbstract.tif
- RevisedSupplementarytable.docx
- SupplementaryFigure1.tif
- Supplementarymaterials.pdf